Morphological integration and serial homology: a case study of the cranium and anterior vertebrae in salamanders

Running title: – Integration and serial homology in salamanders

Aleksandar Urošević[1], Maja Ajduković[1], Jan W. Arntzen[2], Ana Ivanović[2,3]

[1] University of Belgrade, Institute for Biological Research "Siniša Stanković" - National Institute of Republic of Serbia, Belgrade, Serbia

[2]Naturalis Biodiversity Center, Leiden, The Netherlands

[3] University of Belgrade, Institute of Zoology, Faculty of Biology, Belgrade, Serbia

Corresponding author: Aleksandar Urošević, University of Belgrade, Institute for Biological Research "Siniša Stanković" - National Institute of Republic of Serbia, Belgrade, Serbia, email: aurosevic@ibiss.bg.ac.rs

Keywords: axial skeleton, modularity, Salamandridae, serial homology, skull

Abstract

Serial homology or the repetition of equivalent developmental units and their derivatives is a phenomenon encountered in a variety of organisms, with the vertebrate axial skeleton as one of the most notable examples. Serially homologous structures can be viewed as an appropriate model-system for studying morphological integration and modularity, due to the strong impact of development on their covariation. Here, we explored the pattern of morphological integration of the cranium and the first three serially homologous structures (atlas, first and second trunk vertebrae) in salamandrid salamanders, using micro-CT scanning and 3D geometric morphometrics. We explored the integration between structures at static and evolutionary levels. Effects of allometry on patterns of modularity were also taken into account. At the static level (within species), we analyzed inter-individual variation in shape to detect functional modules and intra-individual variation to detect developmental modules. Significant integration (based on inter-individual variation) among all structures was detected and allometry is shown to be an important integrating factor. The pattern of intra-individual, asymmetric variation indicates statistically significant developmental integration between the cranium and the atlas and between the first two trunk vertebrae. At the evolutionary level (among species), the cranium, atlas and trunk vertebrae separate as different modules. Our results show that morphological integration at the evolutionary level coincides with morphological and functional differentiation of the axial skeleton, allowing the more or less independent evolutionary changes of the cranial skeleton and the vertebral column, regardless of the relatively strong integration at the static level. The observed patterns of morphological integration differ across levels, indicating different impacts of developmental and phylogenetic constraints and functional demands.

Introduction

Serial homology, which denotes relationships among iterating series of equivalent developmental units and their derivatives, is widespread in the animal kingdom (Kuratani, 2009). Examples of serially homologous structures in vertebrates include vertebrae (Carapuco, Novoa, Bobola & Mallo, 2005), teeth (Gómez-Robles & Polly, 2012) and limbs (Young & Hallgrímsson, 2005). The underlying developmental program of serially homologous structures is duplicated and then becomes expressed at a different time and in a different location (Hall, 1995). Due to the shared developmental pathways, serially homologous structures tend to strongly co-vary (Cowley & Atchley, 1990; Young & Hallgrímsson, 2005; Wagner, Pavlicev & Cheverud, 2007; Jones, Benitez, Angielczyk & Pierce, 2018). It may therefore be expected that serially homologous structures are highly integrated, unless a functional differentiation occurred ('parcellation', sensu Wagner & Altenberg, 1996).

Vertebrae are derived from primary segmental modules in embryos, the somites (Kuratani, 2009). The process of somitogenesis involves the segmentation of paraxial mesoderm and occurs during early mesoderm differentiation (Palmeirim, Henrique, Ish-Horowicz & Pourquié, 1997; Pourquié, 2003). The first five somites are involved in the formation of the occipital region of the skull, while others give rise to the vertebral column (Kuratani, 2009; Hirasawa & Kuratani, 2015). The identity of the vertebrae is determined during the phylotypic stage of development, via expression of *Hox* genes along the anterior-posterior axis (Krumlauf, 1994; Aulehla & Pourguié, 2010; Mallo, Wellik & Deschamps, 2010; Hirasawa & Kuratani, 2015). For instance, the *Hoxc6* gene is responsible for the cervico–thoracic boundary in amniotes (Burke, Nelson, Morgan & Tabin, 1995; Ohya, Kuraku & Kuratani, 2005; Kuratani, 2009).

The vertebral column in *Ichthyostega*, the early tetrapod taxa, is differentiated into the cervical, thoracic, lumbar, sacral and caudal regions (Ahlberg, Clack & Blom, 2005). Such adaptive regionalization of the vertebral column is, to some extent, present in all tetrapods (Woltering, 2012). It should be noted that in some groups lineage-specific adaptations occur, such as the urostyle in frogs (Emerson, 1985), the carapace in turtles (Nagashima et al., 2012), extended ribs in *Draco* lizards (Colbert, 1967), or the extreme body elongation with secondary de-regionalization in snakes (Woltering, 2012; Head & Polly, 2015). The vertebral column in tailed amphibians is less regionally differentiated. There is one cervical vertebra (atlas) that

articulates with the skull followed by a series of rib-bearing vertebrae. As all vertebrae have similar morphology and there is no differentiation on thoracic (rib-bearing) and lumbar region, this region is traditionally denoted as “trunk region”. The sacral region is consisting of one sacral vertebra followed by a several postsacral vertebrae and the caudal vertebrae (Figure 1). The vertebral column of tailed amphibians is susceptible to variation in vertebrae number, due to the evolutionary process of body shortening and elongation which are related to locomotor constraints and ecology (Arntzen, Beukema, Galis & Ivanović, 2015; Slijepčević, Galis, Arntzen & Ivanović, 2015).

Repeated anatomically homologous structures can be viewed as good model-systems for studying modularity because they usually share a common plan with some quantitative and qualitative differences between the members of the series (Gómez-Robles & Polly, 2012). Until now, studies of morphological integration and modularity were mostly based on patterns of integration between modules within complex structures, such as the cranium, or on structures with matching symmetries such as insect wings or mandibles (Cheverud, 1982; Debat, Alibert, David, Paradis & Auffray, 2000; Klingenberg & Zaklan, 2000; Klingenberg, Mebus & Auffray, 2003; Ivanović & Kalezić, 2010; Jojić, Blagojević & Vujošević, 2011). Studies of morphological integration between separate, serially homologous structures are scarce except for mammals (Young & Hallgrímsson, 2005; McCane & Kean, 2011; Gómez-Robles & Polly, 2012). The modularity of the mammalian vertebral column coincides with patterns of regional differentiation and is influenced by developmental and functional constraints (Randau & Goswami, 2017). Empirical studies indicated that morphological evolution of the mammalian vertebral column was mostly related to function, i.e. locomotor constraints and ecology (Galis et al., 2014; Jones et al., 2018).

We employed micro-CT scanning and 3D geometric morphometrics to analyze the shape of the cranium along with the atlas and first two trunk vertebrae in salamandrid salamanders (Figure 1). The atlas and first two trunk vertebrae were studied to ensure that homologous structures were compared, also when species had different numbers of trunk vertebrae. Specifically, we tested (1) if the pattern of morphological integration coincides with morphological differentiation of the vertebrae, expecting the highest integration between structures within the same region and similar function (i.e. the trunk vertebrae), (2) if adjacent structures are more strongly integrated than separated ones, and (3) we explored morphological

integration at static and evolutionary levels, and tested for the congruence in morphological covariation between them. More specifically, the patterns of integration within a single homogenous sample (a set of individuals of the same species at the same ontogenetic stage), denoted as an example of static integration, can be studied from the functional and developmental point of view. As interaction between developmental pathways usually leads to covariation in fluctuating asymmetry (Klingenberg & Zaklan, 2000), the covariation of intra-individual, asymmetric components of shape variation reflects developmental integration (Klingenberg, 2003; 2005). The pattern of integration across species, denoted as evolutionary integration, takes phylogenetic relationships into account (Klingenberg, 2014). Therefore, we explored developmental and functional integration at the static level and compered the observed patterns with the pattern of integration among species (evolutionary integration) to detect possible roles of developmental and functional constraints in the evolution of the vertebral column of salamandrid salamanders.

Material and methods

We produced three-dimensional (3D) surface models of the cranium, the atlas and the first and second trunk vertebrae for 241 ethanol-preserved adult salamanders of both sexes, representing 17 species and five genera in the family Salamandridae from the collections of the Naturalis Biodiversity Center and the University of Belgrade, Institute for Biological Research "Siniša Stanković" - National Institute of Republic of Serbia (Appendix I). Salamanders were scanned individually with a Skyscan 1171 micro-computed tomography (CT)-scanner at a resolution of 26.1 μm, under optimized settings (59 kV, 0.7 rotation step, 145 ms exposure time). The gathered data were processed with SkyScanCTAnalyser v.1 software under a marching cube algorithm. The configuration of 35 landmarks for the cranium and 14 landmarks for the atlas and first two trunk vertebrae (Figure 2) was digitized on the surface models using Landmark IDAV v.3.6 software (http://graphics.idav.ucdavis.edu/research/EvoMorph). Brief anatomical descriptions are given in Appendix II.

Extraction of shape variables for static and evolutionary integration

Generalized Procrustes Analysis was employed to obtain a matrix of shape coordinates for each of the analyzed structures separately (Rohlf & Slice, 1990; Dryden & Mardia, 1998). The Procrustes superimposition of the original landmark configurations and their mirror images was used to decompose the total shape variation into symmetric and asymmetric variation among individuals (Klingenberg, Barluenga & Meyer, 2002). Both components were kept separate in downstream analyses. Centroid Size (CS) was calculated as a measure of size (Zelditch, Swiderski & Sheets, 2012).

Shape variables for static integration

For the estimation of measurement error, static allometry and shape variables for static integration we selected the genus of aquatic salamanders *Triturus*. This is a monophyletic group here represented by seven species and a large sample size (N=139).

Measurement error was quantified by repeating the landmark acquisition. The level of small, random departures from ideal symmetry, known as fluctuating asymmetry was quantified by a Procrustes ANOVA (Klingenberg & McIntyre, 1998; Klingenberg et al., 2002). The mean square values of FA were compared to those of the measurement error (Klingenberg, 2015). The results showed that FA largely exceeded measurement error (Appendix III), and therefore the asymmetric component can be used in the further analyses. To assess static allometry, we employed a multivariate regression of shape (pooled-within species) on log-transformed CS (Klingenberg, 1996; Monteiro, 1999). Statistical significance was determined by a permutation test (Klingenberg, 2011). For the symmetric component of variation, the static allometry was statistically significant (Appendix IV) and the residuals from multivariate regression were used as the non-allometric component of shape variation. For the asymmetric shape component, the regressions were not statistically significant and the subsequent analyses on the asymmetric shape component were done on shape variables without correction for allometry.

Shape variables for evolutionary integration

A phylogenetic tree derived from nuclear and mitochondrial DNA sequences was lifted from a time calibrated phylogenetic tree for the family Salamandridae, trimmed to just include the studied species and with branching orders for within the genera *Lissotriton* and *Triturus* fitted by

interpolation (Figure 3, data from Pabijan et al., 2015; Pabijan, Zieliński, Dudek, Stuglik & Babik, 2017; Veith, Bogaerts, Pasmans & Kieren, 2018; Wielstra, McCartney-Melstad, Arntzen, Butlin & Shaffer, 2019). We then reconstructed character states at each of the internal nodes of the phylogeny under the criterion of squared-change parsimony (Maddison, 1991), with branch lengths scaled according to the estimated divergence time (Klingenberg & Gidaszewski, 2010). The strength of phylogenetic signal was estimated with a permutation approach against the null hypothesis of no phylogenetic structure (Klingenberg & Gidaszewski, 2010). This approach has been criticized on the ground that estimated phylogenetic signal changes regarding trait variation and the increasing number of trait dimensions (Adams, 2014). Although the proposed alternative statistics have somewhat higher statistical power, the two methods are regarded as similar and yield congruent results, especially for data that are not corrected for allometry (Pearson, Groves & Cardini, 2015). Because we tested for phylogenetic signal on the data without allometric correction with good sample sizes and a relatively small number of landmark points, we conclude that the employed method was adequate for our dataset. The shape variables, represented by the phylogenetically independent contrasts, were estimated as weighted differences of values for sister nodes (Felsenstein, 1985; Garland, Harvey & Ives, 1992; Rohlf, 2001). Principal component analysis (PCA) and superimposition of the phylogenetic tree in the morphospace defined by the first two PC-axes was done to visualize the relationship between morphological disparity and phylogeny in 'phylomorphospace'.

Evolutionary allometry was assessed by a multivariate regression of phylogenetically independent contrasts of shape on independent contrasts of size (Figueirido, Serrano-Alarcón, Slater & Palmqvist, 2010; Perez, Klaczko, Rocatti & dos Reis, 2011). The level of evolutionary allometry was statistically significant in all cases (Appendix IV), and accounted for relatively large proportion (16.5% -19.8%) of the total shape variation observed. The residuals from the multivariate regression of phylogenetically independent contrasts were used as non-allometric component for evolutionary integration (Figueirido et al., 2010; Perez et al., 2011; Klingenberg & Marugán-Lobón, 2013).

Analyses of morphological integration

Morphological integration between the structures was assessed by Two-block Partial Least Squares (PLS) analysis based on a singular value decomposition of the matrix of covariances between the two sets of variables (Bookstein, 1991; Rohlf & Corti, 2000; Young & Hallgrímsson, 2005). The 'separate-subsets' PLS-approach (Klingenberg, 2009) can test covariation between two different sets of landmarks, for which separate Procrustes superimposition were conducted (Bastir & Rosas, 2005; Mc Cane & Kean, 2011; Parsons et al., 2011; Neaux, Guy, Gilissen, Coudyzer & Ducrocq, 2013). A multivariate generalization of Pearson's correlation coefficient (RV) was used as a measure of association between the structures (Escoufier, 1973). The covariation was assessed by a permutation test against the null hypothesis of total independence (Good, 2000; Manly, 2007; Klingenberg, 2009; 2011).

To assess the morphological integration at the static level, we performed pairwise PLS-analyses between the cranium, the atlas and the first and second trunk vertebrae on the covariance matrices (symmetric component of shape variation, pooled-within species). Since allometry can encompass a large amount of overall shape variation and thus may substantially contribute to the shape integration (Zelditch & Fink, 1995; Rosas & Bastir, 2004; Klingenberg, 2009), the same analyses were performed on the non-allometric component of shape variation. Accordingly, we tested integration on the asymmetric component of shape variation, to which we applied the Bonferroni correction for multiple comparisons.

PLS-analysis on the independent contrasts of the cranium, atlas, the first and second trunk vertebrae was used to assess evolutionary shape covariation (Klingenberg & Marugán-Lobón, 2013). In order to estimate possible effects of evolutionary allometry, we also performed PLS-analysis on the non-allometric component under Bonferroni correction.

In order to compare covariation patterns between the static and evolutionary levels, we compared the angles of the trajectories of the main PLS-axes for the analyses between each pair of the structures, both prior and after the correction for allometry. The vectors between PLS-analyses done on symmetric and asymmetric components of shape variation were not compared since they are perpendicular in the shape tangent space. The statistical significance of the angles between vectors was tested against the null hypothesis that the vectors have random directions in the

shape tangent space (Li, 2011; Klingenberg & Marugán-Lobón, 2013). All shape analyses were carried out with MorphoJ software version 1.06c (Klingenberg, 2011).

Results

Static integration

Static integration for the symmetric component of shape variation was low to intermediate but statistically highly significant between all structures. The strongest integration was found for the first and second trunk vertebrae (Table 1, Figure 4). For the static integration between the cranium and the atlas, the first, second and third PLS-axes account for 45.8%, 15.6% and 10.7% of the observed variation, respectively, and were statistically significant in all cases ($p<0.01$). The results are illustrated in Supporting information Figure S1. For the static integration between the atlas and the first trunk vertebra the first and second PLS-axes accounted for 64.8% and 15.1% of the observed variation, respectively and were statistically significant ($p<0.0001$). The changes along the first and second PLS-axes are shown in Supporting information Figure S1. For the first and second trunk vertebrae, PLS-axes accounted for 59.5% and 14.4% of the observed variation, respectively (significant at $p<0.0001$ in both cases). The shape changes of both vertebrae were similar and are shown in Supporting information Figure S1. Static integration after correction for allometry (non-allometric shape variation) was slightly lower (Table 1, Figure 4) and was statistically significant in all cases. However, for the non-allometric static integration of the cranium and the atlas, the signal over the first PLS-axis was not statistically significant (24.7% of total shape covariation, $p>0.05$).The remaining two axes accounted for 24.0% and 16.0%, respectively (significant at $p<0.0001$ in both cases), indicating a relatively weak integration of the cranium and the atlas. Static integration for the asymmetric component of shape variation was relatively low in all cases and only statistically significant for the cranium and the atlas, the atlas and the second trunk vertebra and the first and second trunk vertebrae (Table 1, Figure 4). For the cranium and the atlas, the first three PLS-axes described 32.07%, 20.51% and 12.83% of the total shape covariation, respectively (significant at $p<0.05$ in all cases). Shape changes along the PLS-axes are shown in Supporting information Figure S1. For the first and second trunk vertebrae, the first three PLS axes account for 36.9%, 23.4% and

16.4% of the total shape covariation, respectively (significant at $p<0.01$ in all cases) with corresponding changes represented in Supporting information Figure S2.

Evolutionary integration

Phylogenetic signal was statistically significant for size and shape of the cranium, the atlas and the first and second trunk vertebrae ($p<0.001$ in all cases). Among-species variation in cranium shape is shown in Figure 5A. The first and second PC-axes explain 28.2% and 16.0% of the overall variation in cranium shape, respectively. Plotting the species phylogenetic relationships onto the morphological profile yielded a gradient from *Neurergus crocatus* and the genus *Lissotriton* to *Triturus dobrogicus* over the first axis and from *N. crocatus* plus *T. marmoratus* and *T. pygmaeus* to the genus *Lissotriton* over the second axis (Figure 5A). The shape changes along the first axis correspond to a gradient from shorter and wider crania (especially in the posterior parts) and a shortened occipital region to more elongated and narrower crania with an elongated occipital region. The shape changes along the second axis correspond to a gradient from crania with narrow squamosals and quadrates, elongated premaxillae, maxillae and occipital region, to crania with widened squamosals and quadrates, compressed premaxillae, maxillae and occipital regions. For the atlas the explained among-species variation over the first and second PC-axes was 51.6% and 18.6%, respectively (Figure 5B). The inferred shape changes suggest a dichotomy for *Calotriton asper* and the genus *Triturus* versus the genera *Ichthyosaura*, *Lissotriton*, *Neurergus* and *Ommatotriton* along the first axis. The shape changes along the second axis correspond to a gradient from *T. cristatus*, *T. dobrogicus* and *T. macedonicus* to *T. marmoratus* and *C. asper*, with the remainder of the species taking intermediate positions. The shape changes along the first axis correspond to a gradient from a slightly wider atlas with shortened anterior and elongated posterior parts, to a slightly narrower atlas with elongated anterior and compressed posterior parts. The shape changes along the second axis describe a slightly narrower atlas with the dorsal tip of the vertebra positioned posteriorly to a wider atlas with the dorsal tip positioned anteriorly. For the first trunk vertebrae the explained variation over the first and second PC-axes was 41.0% and 15.5%, respectively (Figure 5C). The bivariate plot displays a gradient from *T. cristatus* to *L. boscai* and *L. helveticus* along the first axis and a gradient from *L. italicus, L. montandoni* and *L. vulgaris* to *C. asper, T. marmoratus* and *T. pygmaeus*, with the remainder of species at intermediate positions at the second axis. The shape changes along the first axis correspond to a gradient from elongated and dorso-ventrally

compressed vertebrae to shortened and dorso-ventrally expanded (i.e. taller) vertebrae. The second axis displays a shape gradient for trunk vertebrae with elongated anterior and compressed posterior parts to vertebrae with shortened anterior and expanded posterior parts. Finally, for the second trunk vertebra the explained variation over the first and second PC-axes was 44.5% and 14.5%, respectively (Figure 5D), with a gradient from *T. cristatus* and *T. dobrogicus* to *L. helveticus* along the first axis, and from *L. italicus*, *L. montandoni* and *L. vulgaris* to *C. asper* and *T. marmoratus* along the second axis. The inferred shape changes are largely similar to those described for the first trunk vertebra.

The evolutionary integration was not statistically significant between cranium and atlas and between cranium and the first trunk vertebra, but it was significant for the other comparisons (Table 2). It was particularly strong between the first and second trunk vertebrae (Table 2, Figure 4). For the evolutionary integration between atlas and first trunk vertebra, the first and second PLS-axes account for 50.5% and 35.0% of the observed variation, respectively, and for the first and second trunk vertebrae these proportions were 47.6% and 38.4% ($p<0.05$ in all cases). Corresponding changes are presented in Supporting information Figure S3. Although allometry accounts for a large proportion of shape variation among species (Appendix IV), the allometry had little effect on the RV-coefficients for evolutionary integration. Among adjacent structures, the non-allometric evolutionary integration was statistically significant only for the first and second trunk vertebrae (Table 2, Figure 4). The first and second PLS-axes accounted for 50.0% and 33.4% of the total shape variation for integration ($p<0.01$ in all cases).

Comparison of integration across levels

Angles between the vectors of the corresponding PLS-axes for the first and second block are presented in Table 3. Most vectors between the corresponding PLS-axes are divergent, the only two cases in which complementary vectors for the first axis were detected for both blocks is for the integration between cranium and atlas, and for the first and second trunk vertebrae.

Discussion

At the static level, a weak but statistically significant integration was found between all studied structures with the strongest signal between the two adjacent trunk vertebrae. In homologous structures such as tetrapod limbs, functional diversification between the front and hind limbs can

reduce the overall strength of integration (Young & Hallgrímsson, 2005). In the case of the atlas vs. the trunk vertebrae, different functional roles could lead to a reduced integration, whereas the morphologically and functionally similar first and second trunk vertebrae remained more strongly integrated. As we noted, studies on morphological covariation and integration between the cranial region and cervical vertebrae are scarce. Morphological covariation between the cranium and cervical vertebrae has been found in primates (humans) at the developmental and functional levels (Solow & Sandham, 2002; Mc Cane & Kean, 2011). That craniovertebral integration, which has now been observed in salamandrids, could indicate that this type of integration is widespread among tetrapods.

The static integration was somewhat less pronounced after removal of the allometric component of shape variation. This is in line with the classic interpretation of allometry as an integrating factor (Zelditch & Fink, 1995; Hallgrímsson et al., 2006; Klingenberg, 2009, but see Ivanović & Kalezić, 2010). However, the static allometry accounted for a relatively low proportion of the total shape variation and the correction for allometry did not actually disrupt the existing pattern of shape integration, it only lessened its strength.

The covariation of the asymmetric component of shape variation is usually influenced by developmental (Klingenberg & McIntyre, 1998; Klingenberg et al., 2002) or functional/developmental relationships (Cheverud, 1995; Marroig & Cheverud, 2001; Ivanović & Kalezić, 2010). All vertebrae and some elements of the neurocranium originate from the paraxial mesoderm. The occipital region and the consecutive vertebrae have the same origin as a result of somite segmentation and re-segmentation (Ewan & Everett, 1992; Piekarski & Olsson, 2014). However, somite differentiation and the formation of vertebrae occur during early development, after which their ontogenetic trajectories are more or less separated. Despite a different origin of the occipital region, which is formed by anterior somites, the cranium is a separate, well integrated structure (Ivanović & Kalezić, 2010). The atlas is functionally associated with the cranium, whereas the first and second trunk vertebrae are involved in locomotion (Omura et al., 2015). Strong integration between the first two trunk vertebrae as well as their integration with the cranium (and not with the atlas) can be explained by their specific functional role. Musculature supporting the pectoral girdle (the *m. thoraciscapularis* and *m. dorso humeralis-oblique posterior*) arises from the first two trunk vertebrae (Francis, 1934). The cranium and trunk vertebrae are functionally connected by the *m. levator mandibulae anterior*,

m. rectus capitis posterior and *m. intertransversarius capitis inferior* which arise from the skull and insert on the first and second trunk vertebrae, or vice versa (Francis, 1934). Under reference to their developmental and functional relationship, the static integration pattern of the vertebrae could be explained by joint developmental and functional factors.

The observed patterns of evolutionary integration suggest that the cranium and the vertebral column are to be viewed as separate evolutionary modules. After the correction for evolutionary allometry, morphological integration remained well supported in only a few cases (namely the cranium vs. the second trunk vertebra and the first vs. second trunk vertebrae). It has been suggested that evolutionary allometry is not the main determinant of evolutionary integration (Klingenberg & Marugán-Lobón, 2013). However, in some cases, evolutionary allometry can explain a large proportion of shape variation, and the residual variation correlates with phylogeny (Jones, 2015). In the case of the salamander's axial skeleton, the support for integration of the atlas and the first trunk vertebra disappeared after a correction for allometry and only the first and second trunk vertebrae remained strongly integrated, which leaves the cranium, the atlas and the set of trunk vertebrae as three distinct evolutionary modules. It also confirms that allometry is an important integrating factor even in serially homologous structures such as vertebrae. The divergent vectors of the PLS-analyses at the static and evolutionary level also confirm that the patterns of static and evolutionary integration are different.

The morphological evolution of the vertebral column in salamandrid salamanders is influenced by the general pattern of body elongation or shortening (Arntzen et al., 2015; Urošević, Slijepčević, Arntzen & Ivanović, 2016). The evolution of the cranium is more complex, with independent changes in the cranial roof bones leading to convergence in cranial shape (Ivanović & Arntzen, 2018). Our results on morphological integration of the cranium and anterior parts of the vertebral column indicate that dissociation of elements at the evolutionary level facilitates their independent evolution, whereas shared developmental factors and functional constraints strengthen the overall integration patterns at the individual and taxon level. Allometry serves as a common integrating factor within and across taxa. Such a pattern also indicates that natural selection produced the decoupled morphological integration, in salamandrid salamanders allowing for the relatively independent evolutionary change of the cranium and the vertebral column. More studies on functional differentiation and integration and

allometry of homologous structures across different taxa are needed to further explore patterns of size and shape covariation in serial homology.

Acknowledgements

We would like to thank Emma Sherratt and the anonymous reviewer for constructive comments that improved the quality of the manuscript, Andrea Cardini for advice on statistical methods and Esther Dondorp at Naturalis Biodiversity Center, Leiden, for collection management. The study was funded by the Serbian Ministry of Education and Science (grant no. 173043 to AU, MA and AI) and by a Naturalis Temminck Fellowship and grants from SyntheSys (NL-TAF 3082, 3926) to AI.

References

Adams, D. C. (2014). A generalized K statistic for estimating phylogenetic signal from shape and other high-dimensional multivariate data. Systematic Biology, 3(5), 685–697. doi: 10.1093/sysbio/syu030

Ahlberg, P. E., Clack, J. A, & Blom, H. (2005). The axial skeleton of the Devonian tetrapod *Ichthyostega*. *Nature* 437:137–140. doi: 10.1038/nature03893

Arntzen, J. W., Beukema, W., Galis, F., & Ivanović, A. (2015). Vertebral number is highly evolvable in salamanders and newts (family Salamandridae) and variably associated with climatic parameters. *Contributions to Zoology*, 84, 85–113. doi: 10.1163/18759866-08402001

Aulehla, A., & Pourguié, O. (2010). Signaling gradients during paraxial mesoderm development. *Cold Spring Harbor Perspectives in Biology*, 2, a000869. doi: 10.1101/cshperspect.a000869

Bastir, M., & Rosas, A. (2005). Hierarchical nature of morphological integration and modularity in the human posterior face. *American Journal of Physical Anthropology*, 128, 26–34. doi: 10.1002/ajpa.20191

Bookstein, F. L. (1991). *Morphometric tools for landmark data: geometry and biology*. Cambridge, UK: Cambridge University Press.

Burke, A. C., Nelson, C. E., Morgan, B. A., & Tabin, C. (1995). Hox genes and the evolution of vertebrate axial morphology. *Development*, 121, 333–346. PubMed: 7768176

Carapuco, M., Novoa, A., Bobola, N., & Mallo, M. (2005). Hox genes specify vertebral types in the presomitic mesoderm. *Genes & Development*, 19, 2116–2121. doi: 10.1101/gad.338705

Cheverud, J. M. (1982). Phenotypic, genetic, and environmental morphological integration in the cranium. *Evolution*, 36, 499–516. doi:10.2307/ 2408096

Cheverud, J. M. (1995). Morphological integration in the saddle-back tamarin (*Saguinus fuscicollis*) cranium. *The American Naturalist*, 145, 63–89. doi: 10.1086/285728

Colbert, E.H. (1967) Adaptations for gliding in the lizard *Draco*. *American Museum Novitates*, 1967, 1-20. uri: http://hdl.handle.net/2246/3081

Cowley, D. E. & Atchley, W. R. (1990). Development and quantitative genetics of correlation structure among body parts of *Drosophila melanogaster*. *The American Naturalist*, 135, 242–268. doi: 10.1086/285041

Debat, V., Alibert, P., David, P., Paradis, E., & Auffray, J.-C. (2000). Independence between developmental stability and canalization in the skull of the house mouse. *Proceedings of the Royal Society of London B: Biological Sciences*, 267, 423–430. doi: 10.1098/rspb.2000.1017

Dryden, I. L., & Mardia, K. V. (1998). *Statistical Shape Analysis*. New York, NY: Wiley.

Emerson, S. B. (1985). Jumping and leaping. In M. Hildebrand, D. M. Bramble, L. F. Karel & D. B. Wake (Eds.), *Functional Vertebrate Morphology* (pp. 58–72). Cambridge, MA: Harvard University Press.

Escoufier, Y. (1973). Le traitement des variables vectorielles. *Biometrics*, 29, 751–760. doi: 10.2307/2529140

Ewan, K. B. R., & Everett, A. W. (1992). Evidence for resegmentation in the formation of the vertebral column using the novel approach of retroviral-mediated gene transfer. *Experimental Cell Research*, 198, 315–320. doi: 10.1016/0014-4827(92)90385-L

Felsenstein, J., (1985). Phylogenies and the comparative method. *The American Naturalist*, 125, 1–15. doi: 10.1086/284325

Figueirido, B., Serrano-Alarcón, F. J., Slater, G. J., & Palmqvist, P. (2010). Shape at the cross-roads: homoplasy and history in the evolution of the carnivoran skull towards herbivory. *Journal of Evolutionary Biology*, 23, 2579–2594. doi: 10.1111/j.1420-9101.2010.02117.x

Francis, E. B. T., (1934). *The anatomy of the Salamander*. Oxford, UK: Clarendon Press.

Galis, F., Carrier, D. R., Van Alphen, J., Van der Mije, S. D., Van Dooren, T. J. M., Metz, J. A. J., & ten Broek, C. M. A. (2014). Fast running restricts evolutionary change of the vertebral column in mammals. *PNAS*, 111(31), 11401–11406. doi: 10.1073/pnas.1401392111

Garland, T. Jr., Harvey, P.H., & Ives, A. R. (1992). Procedures for the analysis of comparative data using phylogenetically independent contrasts. *Systematic Biology*, 41, 18–32. doi: 10.1093/sysbio/41.1.18

Good, P. (2000). *Permutation tests: a practical guide to resampling methods for testing hypotheses*. 2nd ed. New York, NY: Springer.

Gómez-Robles, A., & Polly, D. P. (2012). Morphological integration in the hominin dentition: Evolutionary, developmental, and functional factors. *Evolution*, 66, 1024-1043. doi: 10.1111/j.1558-5646.2011.01508.x

Hall, B. K. (1995). Homology and embryonic development. *Evolutionary Biology*, 28, 1-36. https://doi.org/10.1007/978-1-4615-1847-1_1

Hallgrímsson, B., Brown, J. J. Y., Ford-Hutchinson, A. F., Sheets, H. D., Zelditch, M. L., & Jirk, F. R. (2006).The brachymorph mouse and the developmental genetic basis for canalization and morphological integration. *Evolution & Development*, 8, 61–73. doi: 10.1111/j.1525-142X.2006.05075.x

Head, J. J., & Polly, D. P. (2015). Evolution of the snake body form reveals homoplasy in amniote Hox gene function. Nature, 520, 86–89. doi: 10.1038/nature14042

Hirasawa, T., & Kuratani, S. (2015). Evolution of the vertebrate skeleton: morphology, embryology, and development. *Zoological Letters*, 1, 2. doi: 10.1186/s40851-014-0007-7

Ivanović, A., & Kalezić, M. L. (2010). Testing the hypothesis of morphological integration on a skull of a vertebrate with a biphasic life cycle: a case study of the alpine newt. *Journal of Experimental Zoology Part B-Molecular and Developmental Evolution*, 314, 527–538. doi: 10.1002/jez.b.21358

Ivanović, A., & Arntzen, J. W. (2018). Evolution of skull shape in the family Salamandridae (Amphibia: Caudata). *Journal of Anatomy*, 232, 359-370. doi: 10.1111/joa.12759

Jojić, V., Blagojević, J., & Vujošević, M. (2011). B chromosomes and cranial variability in yellow necked field mice (*Apodemus flavicollis*). *Journal of Mammalogy*, 92, 396–406. doi:10.1644/10-MAMM-A-158.1

Jones, K. E. (2015). Evolutionary allometry of lumbar shape in Felidae and Bovidae. *Biological Journal of the Linnean Society*, 116(3), 721–740. doi: 10.1111/bij.12630

Jones, K. E., Benitez, L., Angielczyk, K. D., & Pierce, S. E. (2018). Adaptation and constraint in the evolution of the mammalian backbone. *BMC Evolutionary Biology*, 18, 172. doi: 10.1186/s12862-018-1282-2

Klingenberg, C. P. (1996). Multivariate allometry. In L. F. Marcus, M. Corti, A. Loy, G. J. P. Naylor, & D. E. Slice (Eds.), *Advances in morphometrics* (pp. 23–49). New York, NY: Plenum Press.

Klingenberg, C. P. (2003). Developmental instability as a research tool: using patterns of fluctuating asymmetry to infer the developmental origins of morphological integration. In M. Polak (Ed.), *Developmental instability: causes and consequences* (pp. 427–442). New York, NY: Oxford University Press.

Klingenberg, C. P., (2005). Developmental constraints, modules and evolvability. In B. Hallgrímsson & B. K. Hall (Eds.), *Variation* (pp. 219–247). San Diego, CA: Academic Press.

Klingenberg, C. P. (2009). Morphometric integration and modularity in configurations of landmarks: Tools for evaluating a-priori hypotheses. *Evolution & Development*, 11, 405–421. doi: 10.1111/j.1525-142X.2009.00347.x

Klingenberg, C. P. (2011). MorphoJ: an integrated software package for geometric morphometrics. *Molecular Ecology Resources*, 11, 353–357. doi: 10.1111/j.1755-0998.2010.02924.x

Klingenberg, C. P. (2014). Studying morphological integration and modularity at multiple levels: concepts and analysis. *Philosophical Transactions of the Royal Society of London B Biological Sciences*, 369, 20130249. doi: 10.1098/rstb.2013.0249

Klingenberg, C. P. (2015). Analyzing fluctuating asymmetry with geometric morphometrics: concepts, methods, and applications. *Symmetry*, 7, 843–934. doi:10.3390/sym7020843

Klingenberg, C. P., & McIntyre, G. S. (1998). Geometric morphometrics of developmental instability: analyzing patterns of fluctuating asymmetry with Procrustes methods. *Evolution*, 52: 1363–1375. doi: 10.1111/j.1558-5646.1998.tb02018.x

Klingenberg, C. P., & S. D. Zaklan. (2000). Morphological integration between developmental compartments in the *Drosophila* wing. *Evolution*, 54, 1273–1285. doi: 10.1111/j.0014-3820.2000.tb00560.x

Klingenberg, C. P., & Gidaszewski, N. A. (2010). Testing and quantifying phylogenetic signals and homoplasy in morphometric data. *Systematic Biology*, 59, 245–261. doi: 10.1093/sysbio/syp106.

Klingenberg, C. P., & Marugán-Lobón, J. (2013). Evolutionary covariation in geometric morphometric data: analyzing integration, modularity and allometry in a phylogenetic context. *Systematic Biology*, 62, 591–610. doi: 10.1093/sysbio/syt025

Klingenberg, C. P., Barluenga, M., & Meyer, A. (2002). Shape analysis of symmetric structures: quantifying variation among individuals and asymmetry. *Evolution*, 56, 1909–1920. doi: 10.1111/j.0014-3820.2002.tb00117.x

Klingenberg, C. P., Mebus, K., & Auffray, J. -C. (2003). Developmental integration in a complex morphological structure: how distinct are the modules in the mouse mandible? *Evolution & Development*, 5, 522–531. doi: 10.1046/j.1525-142X.2003.03057.x

Krumlauf, R. (1994). Hox genes in vertebrate development. *Cell*, 78, 191–201. doi: 10.1016/0092-8674(94)90290-9

Kuratani, S. (2009). Modularity, comparative embryology and evo-devo: Developmental dissection of evolving body plans. *Developmental Biology*, 332, 61–69. doi: 10.1016/j.ydbio.2009.05.564

Li, S. (2011). Concise formulas for the area and volume of a hyperspherical cap. *Asian Journal of Mathematics & Statistics*, 4, 66–70. doi: 10.3923/ajms.2011.66.70

Maddison, W. P. (1991). Squared-change parsimony reconstructions of ancestral states for continuous-valued characters on a phylogenetic tree. *Systematic Zoology*, 40, 304–314. doi: 10.2307/2992324

Mallo, M., Wellik, D. M., & Deschamps, J. (2010). Hox Genes and regional patterning of the vertebrate body plan. *Developmental Biology*, 344(1), 7–15. doi: 10.1016/j.ydbio.2010.04.024

Manly, B. F. J. 2007. *Randomization, bootstrap and Monte Carlo methods in biology*. Boca Raton (FL): Chapman & Hall/CRC.

Marroig, G., & Cheverud, J. M. (2001). A comparison of phenotypic variation and covariation patterns and the role of phylogeny, ecology and ontogeny during cranial evolution of new world monkeys. *Evolution*, 55, 2576–2600. doi: 10.1554/0014-3820(2001)055[2576:ACOPVA]2.0.CO;2

McCane, B., & Kean, M. R. (2011). Integration of parts in the facial skeleton and cervical vertebrae. *American Journal of Orthodontics and Dentofacial Orthopedics*, 139, e13–e30. doi: 10.1016/j.ajodo.2010.06.016.

Monteiro, L. R. (1999). Multivariate regression models and geometric morphometrics: the search for causal factors in the analysis of shape. *Systematic Biology*, 48, 192–199.

Nagashima, H., Kuraku, S., Uchida, K., Kawashima-Ohya, Y., Narita, Y., & Kuratani, S. (2012). Body plan of turtles: an anatomical, developmental and evolutionary perspective. *Anatomical Science International*, 87, 1–13. doi: 10.1007/s12565-011-0121-y

Neaux, D., Guy, F., Gilissen, E., Coudyzer, W., & Ducrocq, S. (2013).Covariation between midline cranial base, lateral basicranium, and face in modern humans and chimpanzees: a 3D geometric morphometric analysis. *Anatomical Record*, 296, 568–579. doi: 10.1002/ar.22654

Ohya, Y. K., Kuraku, S., & Kuratani, S. (2005). Hox code in embryos of Chinese Soft-Shelled Turtle *Pelodiscus sinensis* correlates with the evolutionary innovation in the turtle. *Journal of experimental zoology (Mol Dev Evol)*, 304B, 107–118. doi: 10.1002/jez.b.21027

Omura, A., Ichiro Ejima, K., Honda, K., Anzai, W.,Taguchi, Y., Koyabu, D., & Endo, H. (2015). Locomotion pattern and trunk musculoskeletal architecture among Urodela. *Acta Zoologica*, 96, 225-235. doi: 10.1111/azo.12070

Pabijan, M., Zieliński, P., Dudek, K., Chloupek, M., Sotiropoulos, K., Liana, M., & Babik, W. (2015). The dissection of a Pleistocene refugium: phylogeography of the smooth newt, *Lissotriton vulgaris*, in the Balkans. *Journal of Biogeography*, 42, 671–683. doi: 10.1111/jbi.12449

Pabijan, M., Zieliński, P., Dudek, K., Stuglik, M., & Babik, W. (2017). Isolation and gene flow in a speciation continuum in newts. *Molecular Phylogenetics and Evolution*, 116, 1–12. doi: 10.1016/j.ympev.2017.08.003

Palmeirim, I., Henrique, D., Ish-Horowicz, D., & Pourquié, O. (1997) Avian hairy gene expression identifies a molecular clock linked to vertebrate segmentation and somitogenesis. *Cell*, 91, 639–648. doi: 10.1016/s0092-8674(00)80451-1

Parsons T. E., Schmidt E. J., Boughner J. C., Jamniczky H. A., Marcucio R. S., & Hallgrímsson B. (2011). Epigenetic integration of the developing brain and face. *Developmental Dynamics*, 240, 2233–2244. doi: 10.1002/dvdy.22729

Pearson, A., Groves, C., & Cardini, A. (2015). The 'temporal effect' in hominids: Reinvestigating the nature of support for a chimp-human clade in bone morphology. Journal of Human Evolution, 88, 146–159. doi: 10.1016/j.jhevol.2015.06.012

Perez, S. I., Klaczko, J., Rocatti, G., & dos Reis, S. F. (2011). Patterns of cranial shape diversification during the phylogenetic branching process of New World monkeys (Primates: Platyrrhini*). Journal of Evolutionary Biology*, 24, 1826–1835. doi: 10.1111/j.1420-9101.2011.02309.x

Piekarski, N., & Olsson, L. (2014). Resegmentation in the mexican axolotl, *Ambystoma mexicanum*. *Journal of Morphology*, 275(2), 141-152. doi: 10.1002/jmor.20204

Pourquié, O. (2003). The segmentation clock: converting embryonic time into spatial pattern. *Science*, 301, 328–330. doi: 10.1126/science.1085887

Randau, M., & Goswami, A. (2017). Morphological modularity in the vertebral column of Felidae (Mammalia, Carnivora). *BMC Evolutionary Biology*, 17(1), 133. doi: 10.1186/s12862-017-0975-2

Rohlf, F. J. (2001). Comparative methods for the analysis of continuous variables:geometric interpretations. *Evolution*, 55, 2143–2160.

Rohlf, F. J., & Slice, D. E. (1990). Extensions of the Procrustes method for the optimal superimposition of landmarks. *Systematic Zoology*, 39, 40–59. doi: 10.2307/2992207

Rohlf, F. J., & Corti, M. (2000). The use of two-block partial least-squares to study covariation in shape. *Systematic Biology*, 49, 740–753. doi: 10.1080/106351500750049806

Rosas, A., & Bastir, M. (2004). Geometric morphometric analysis of allometric variation in the mandibular morphology of the hominids of Atapuerca, Sima de los Huesos site. *Anatomical Record*, 278A, 551–560. doi: 10.1002/ar.a.20049

Slijepčević, M., Galis, F., Arntzen, J. W., & Ivanović, A. (2015). Homeotic transformations and number changes in the vertebral column of *Triturus* newts. *PeerJ*, 3, e1397. doi: 10.7717/peerj.1397

Solow, B., & Sandham, A. (2002). Cranio-cervical posture: a factor in the development and function of the dentofacial structures. *European Journal of Orthodontics*, 24, 447-456. doi: 10.1093/ejo/24.5.447

Urošević, A., Slijepčević, M., Arntzen J. W., & Ivanović, A. (2016). Vertebral shape and body elongation in *Triturus* newts. *Zoology*, 119, 439–446. doi: 10.1016/j.zool.2016.05.003

Veith, M., Bogaerts, S., Pasmans, F., & Kieren, S. (2018). The changing views on the evolutionary relationships of extant Salamandridae (Amphibia: Urodela). *PLoS ONE*, 13(8), e0198237. doi: 10.1371/journal.pone.0198237

Wagner, G. P., & Altenberg, L. (1996). Complex adaptations and the evolution of evolvability. *Evolution*, 50, 967–976.

Wagner, G. P., Pavlicev, M., & Cheverud, J.M. (2007). The road to modularity. *Nature Reviews Genetics*, 8, 921–931. doi: 10.1038/nrg2267

Wielstra, B., McCartney-Melstad, E., Arntzen, J. W., Butlin, R. K., & Shaffer, H. B. (2019). Phylogenomics of the adaptive radiation of *Triturus* newts supports gradual ecological niche expansion towards an incrementally aquatic lifestyle. *Molecular Phylogenetics and Evolution*, 133, 120–127. doi: 10.1016/j.ympev.2018.12.032

Woltering, J. M. (2012). From lizard to snake; behind the evolution of an extreme body plan. *Current genomics*, 13, 289–299. doi: 10.2174/138920212800793302

Young, N. M., & Hallgrímsson, B. (2005). Serial homology and the evolution of mammalian limb covariation structure. *Evolution*, 59, 2691-2704. doi: 10.1111/j.0014-3820.2005.tb00980.x

Zelditch, M. L, & Fink, W. L. (1995). Allometry and developmental integration of body growth in a piranha, *Pygocentrus nattereri* (Teleostei: Ostariophysi*). Journal of Morphology*, 223, 41–355. doi: 10.1002/jmor.1052230309

Zelditch, M. L., Swiderski, D. L., & Sheets, D. H. (2012). *Geometric morphometrics for biologists: a primer*. San Diego, CA: Elsevier Academic Press.

Figure Legends

Figure 1. Regional differentiation of the vertebral column in salamandrid salamanders. The analyzed structures are marked on the 3D-model of a *Ichthyosaura alpestris* skeleton.

Figure 2. Three-dimensional surface models of the cranium, atlas and the first two trunk vertebrae, with superimposed landmarks. Descriptions for landmarks digitized on each structure are shown in Appendix II.

Figure 3. Phylogenetic relationships of 17 species of salamandrid salamanders figuring in the present study. The tree is compiled from data by Pabijan et al. (2015, 2017), Veith et al. (2018) and Wielstra et al. (2019) (details see text).

Figure 4. Patterns of morphological integration of the cranium and homologous series of vertebrae at static, developmental and evolutionary levels. For the static and evolutionary level patterns are given before and after correction for allometry. C – cranium, A – atlas, I – first trunk vertebra, II – second trunk vertebra. Thin lines represent weak integration (RV<0.5), medium thick lines represent medium integration (0.50<RV<0.75) and thick lines represent strong integration (RV>0.75). Solid lines represent integration between adjacent structures, dashed lines represent integration between separated elements.

Figure 5. Phylomorphospace of the cranium (A), atlas (B), first (C) and second trunk vertebrae (D), over the first and second principal component axis, for the symmetric component of shape variation, allometric component included. The shape changes corresponding to maximal PC-scores are presented as wireframe graphs for dorsal and lateral projection along each axis. Species names are abbreviated as : Casp - *Calotriton asper,* Ialp - *Ichthyosaura alpestris,* Lbos - *Lissotriton boscai,* Lhel - *Lissotriton helveticus,* Lita - *Lissotriton italicus,* Lmon - *Lissotriton montandoni,* Lvul - *Lissotriton vulgaris,* Ooph - *Ommatotriton ophryticus,* Ovit - *Ommatotriton vittatus,* Ncro - *Neurergus crocatus,* Tcar - *Triturus carnifex,* Tcri - *Triturus cristatus,* Tdob - *Triturus dobrogicus,* Tiva - *Triturus ivanbureschi,* Tmac - *Triturus macedonicus,* Tmar -*Triturus marmoratus,* Tpyg - *Triturus pygmaeus.*

Supporting information

Figure S1. Patterns of static integration of the cranium and the atlas (A), atlas and first trunk vertebra (B) and first and second trunk vertebrae (C), with wireframe graphs for dorsal and lateral projections. For each diagram, grey lines with open landmark points represent mean shape, and black lines with solid landmark points represent shape for a PLS-score of 0.1. Shape changes of the cranium and the atlas along the first PLS-axis depict a slight narrowing of the maxillae, an anterio-posterior compression of the occipital region and a widening of the posterior parts of the cranium, with a simultaneous shortening of the anterior parts of the atlas, an anterior shift of the dorsal tip of the vertebrae and the tip of the laminae and a slight widening of the posterior parts of the atlas. The shape changes along the second PLS-axis show a flattening, narrowing and slight elongation of the cranium, a shortening of the occipital region and a widening of squamosals. The simultaneous changes in the atlas include a shortening of the posterior parts of the atlas, a posterior shift of the condylar facets and a widening of the maximal constriction of the atlas. The third PLS-axis describes a slight shortening, widening and increase in height of the cranium, with a simultaneous decrease in height and increase in width of the posterior parts of atlas (Figure A). The shape covariation of the atlas and the first trunk vertebra involves an increase in the length of the atlas, with a posterior shift of the dorsal tip and the tip of the laminae. The simultaneous shape changes in the first trunk vertebra involve a general increase in height, shortening and widening of the vertebra. The shape changes along the second PLS-axis involve a slight elongation and widening of the anterior parts of the atlas and a shortening and narrowing of the posterior parts of the atlas, with a simultaneous increase in height and narrowing of the anterior and posterior parts of the first trunk vertebra (Figure B). The shape changes of the first and second trunk vertebrae are analogous and involve an increase in height, shortening and widening along the first PLS-axis 1 and an elongation in anterior and shortening in posterior parts of the vertebra and elongation of the rib-bearers along the second PLS-axis (Figure C).

Figure S2. Patterns of static integration (the asymmetric component of shape variation) of the cranium and the atlas (A) and the first and second trunk vertebrae (B), with wireframe graphs for

dorsal and lateral projections. For each diagram, grey lines with open landmark points represent mean shape, and black lines with solid landmark points represent shape for a PLS score 0.1, respectively. The first PLS axis for the cranium depicts asymmetric shifts of posterior parts of the cranium and movements in the same direction of pterygoids and rostral regions. Analogous shape changes of the atlas involve an asymmetric shift of the dorsal tip of the atlas, the tip of the laminae and postzygapophysis, and counter-movements of the condylar facets and maximal constriction of the atlas. The shape changes of the cranium along the second PLS axis involve a strong asymmetric curvature of the frontoparietal region and opposite shape changes of pterygoids, squamosals, and occipital region. The shape changes of atlas along the second PLS axis involve anterior-posterior shifts of the anterior edge of condylar facets, lateral shift of posterior tip of the condylar facets and maximum constriction of the atlas and opposite shift of the anterior-most point on atlas. The cranium shape changes along the third PLS axis involve a lateral shift of the rostral region of the cranium, with the opposite shift of pterygoids and squamosals. The analogous shape changes for the atlas involve a lateral shift of the condylar facets and postzygapophysis and a shift of the dorsal tip of the atlas and tip of the laminae and tip of the cotylus in the opposite direction (A). The shape changes along the first PLS axis for the first trunk vertebra describe a lateral shift of prezygapophyses, an opposite shift of rib bearers and lateral shift of neurapophysis, while analogous shape changes on the second trunk vertebra were similar as for the first but of lesser intensity. The shape changes along the second PLS axis involve an anterior-posterior shift of the prezygapophysis and postzygapophysis, lateral shift of the anterior and posterior dorsal tips of the vertebra, and widening/narrowing of the rib bearers. The analogous shape changes of the second trunk vertebra involve an anteroposterior shift of the prezygapophysis and lateral shift of anterior and posterior dorsal tips of the vertebra. The shape changes along the third PLS axis involve an anteroposterior shift of the maximum constriction of the vertebra at the level of transversal processes, lateral shift of the distal tip of the vertebra and rib-bearers and opposite shift of the prezygapophysis. Analogous shape changes of the second trunk vertebra involve an anteroposterior shift of the prezygapophysis and shift in the opposite direction of the maximum constriction of the vertebra at the level of transversal processes and rib-bearers (B).

Figure S3. Patterns of evolutionary integration of the atlas and the first trunk (A) and the first and second trunk vertebrae (B) with wireframe graphs for dorsal and lateral projections. For each diagram, grey lines with open landmark points represent mean shape and black lines with solid black landmark points represent shape for a PLS score 0.1, respectively. The shape changes of atlas along the first PLS axis involve shortening and widening of the posterior parts of atlas and posterior shift of the dorsal tip of the atlas and tip of the laminae. Analogous shape changes of the first trunk vertebra involve shortening of anterior parts and widening of the whole vertebra, with the anterior shift of the rib bearers. The shape changes of atlas along the second PLS axis involve an anterior shift of the dorsal tip of the atlas and tip of the laminae and slight narrowing and decrease in height of the vertebra, while the analogous shape changes of the first trunk vertebra involve elongation and decrease in height with shortening of the rib bearers (A). The shape changes of the first and second trunk vertebrae along the first PLS axis are similar and involve shortening of the anterior parts, widening and elongation of the posterior parts and anterior shift of the rib bearers. The shape changes along the second PLS axis are also similar for the first and second trunk vertebrae and involve flattening, elongation and widening, especially in the region of the maximum constriction of the vertebra at the level of transversal processes, and shortening of the rib bearers (B).

Table 1. RV-correlation coefficients for static integration. Top panel present results for the symmetric component of variation. Above the diagonal are results for the size corrected, non-allometric component of shape variation. The bottom panel represents RV values for the asymmetric component of shape variation. * denote the statistical significance after Bonferroni correction.

Symmetric	Cranium	Atlas	First trunk	Second trunk
Cranium		0.16*	0.18*	0.17*
Atlas	0.19*		0.21*	0.17*
First trunk	0.21*	0.32*		0.47*
Second trunk	0.20*	0.26*	0.54*	
Asymmetric				
Cranium				
Atlas	0.14*			
First trunk	0.13	0.10		
Second trunk	0.13	0.12*	0.14*	

Table 2. RV coefficients for evolutionary integration. Above the diagonal are results for the non-allometric component of shape variation among taxa. * denote the statistical significance after Bonferroni correction.

Independent contrasts	Cranium	Atlas	First trunk	Second trunk
Cranium		0.49	0.47	0.62*
Atlas	0.56		0.56	0.52
First trunk	0.53	0.63*		0.75*
Second trunk	0.66*	0.63 *	0.84*	

Table 3. Angles between the vectors of the corresponding PLS axes, comparison between static and evolutionary integration prior to and after the correction for allometry. Asterisk denotes statistical significance after the permutation test against the null hypothesis that the vectors have random directions. *** $p<0.0001$; ** $p<0.001$; * $p<0.05$.

Component	Comparison	Block 1			Block 2		
		PLS 1	PLS 2	PLS 3	PLS 1	PLS 2	PLS 3
Total shape	Cranium-Atlas	47.199 ***	85.573	75.016	57.531 *	80.464	85.638
	Cranium-I Trunk	74.215	74.424	75.649	62.466 *	73.924	69.076
	Cranium-II Trunk	72.320 *	83.138	81.346	88.771	77.558	77.590
	Atlas - I Trunk	89.879	88.126	78.125	88.822	85.270	74.746
	Atlas - II Trunk	89.719	72.423	89.339	79.949	74.695	86.928
	I trunk - II Trunk	53.713 **	70.826	69.424	61.118 *	83.969	68.818
Non-allometric	Cranium-Atlas	72.752 *	73.368 *	82.044	85.983	70.591	82.954
	Cranium-I Trunk	84.960	88.128	86.093	60.627 *	64.574	80.399
	Cranium-II Trunk	79.597	87.284	85.846	77.988	72.805	82.561
	Atlas - I Trunk	88.019	72.859	84.190	82.405	68.216	86.642
	Atlas - II Trunk	83.874	86.330	69.192	69.178	85.848	88.747
	I trunk - II Trunk	66.849	74.470	70.079	76.290	84.825	77.804

Appendix I

Analyzed sample, with binomial and common species names, sample size and collection numbers. Museum codes are (in alphabetical order): IBISS–Institute for Biological Research ‘Siniša Stanković’ collection, University of Belgrade, Serbia; RenA –Naturalis Biodiversity Centre, Leiden, The Netherlands. NC=sample size per species for cranium; NA= sample size per species for atlas; NI = sample size per species for I trunk vertebra; NII = sample size per species for II trunk vertebra.

Calotriton asper Dugès, 1852, Pyrenean brook salamander, NC=13, NA=13, NI=12, NII=5, RenA.RMNH _39377-39379, RenA.ZMA_4395/a, RenA.ZMA_5640/a,b,c,e,f, RenA.ZMA_6337/c,d, RenA.RMNH_9432/1,2; *Ichthyosaura alpestris* Laurenti, 1768, Alpine newt, NC=9, NA=9, NI=9, NII=9, RenA.RMNH_9310/a,c,e,n, RenA.RMNH_9602/1, IBISS 14a7, IBISS 18a7, IBISS g21699, IBISS g21709; *Lissotriton boscai* Lataste, 1879, Bosca’s newt, NC=15, NA=15, NI=15, NII=15, RenA.RMNH_10463/a,c, RenA.RMNH_39993_93; 39995_92; 39995_95, RenA.RMNH_4135/b,c,e,g, RenA.RMNH_5645/a,b,d, RenA.RMNH_6779/a, RenA.RMNH_9284/c,g; *Lissotriton helveticus*, Razoumovsky, 1789, NC=24, NA=24, NI=24, NII=24, RenA.RMNH_10490/a,b,c; 10490/a,b,c,d; 10490_4m/a,b, RenA.RMNH_8029/183-186; 8029/188-190; 8029/192-195; 8029/197; 8029/199; 8029/204-205; *Lissotriton italicus* Peracca, 1898, Italian newt, NC=9, NA=9, NI=9, NII=9, RenA.ZMA_7659/1-4; 7659/6-7; 7659/11-12; 7659/14; *Lissotriton montandoni* Boulenger, 1860, Carpathian newt, NC=10, NA=10, NI=10, NII=10, RenA.RMNH_6633/a,b,d,f,h,n,s,t, RenA.RMNH_7582/e; *Lissotriton vulgaris* Linnaeus, 1758, Smooth newt, NC=10, NA=10, NI=10, NII=10, RenA.RMNH_5023/a,b; 9521/a,d,g,k,l,m, RenA.ZMA_5599/3,5; *Ommatotriton ophryticus* Berthold, 1846, Northern banded newt, NC=5, NA=5, NI=5, NII=5, RenA.ZMA_9181/3, RenA.ZMA_9193/a,b,c, RenA.ZMA_9194/f; *Ommatotriton vittatus* Gray, 1835, Southern banded newt, NC=4, NA=4, NI=4, NII=4, RenA.ZMA_9340/a,b,c,d; *Neurergus crocatus* Cope, 1862, Yellow-spotted newt, NC=3, NA=3, NI=3, NII=3, RenA.RMNH_39418, RenA.RMNH_39420-39421; *Triturus carnifex* Laurenti, 1768, Italian crested newt, NC=17, NA=17, NI=16, NII=16, RenA.ZMA_9106/474-477, RenA.ZMA_9107/780-783, RenA.ZMA_9108/405-410, RenA.ZMA_9252/318-320; *Triturus cristatus* Laurenti, 1768, Northern crested newt, NC=20, NA=20, NI=19, NII=18, RenA.ZMA_9153/584-593, RenA.ZMA_9167/711-715,757,758, 355,356,359; *Triturus dobrogicus* Kiritzescu, 1903, Danube crested newt, NC=32, NA=32, NI=32, NII=24, RenA.ZMA_9120/846-852, RenA.ZMA_9090/296, RenA.ZMA_9153/427-434, 745, RenA.ZMA_9101/837-843, RenA.ZMA_9141/365, RenA.ZMA_9083/512-514,744; *Triturus ivanbureschi* Arntzen & Wielstra, 2013, Balkan crested newt, NC=14, NA=14, NI=13, NII=11, RenA.RMNH_47200- 47204; 47211-47213, RenA.ZMA_9134/442-445,771,772; *Triturus macedonicus* Karaman, 1922, Macedonian crested newt, NC=17, NA=17, NI=17, NII=14, RenA.ZMA_9085/658-660; 9085/674-676, RenA.ZMA_9118/898-908; *Triturus marmoratus* Latreille, 1800, Marbled newt, NC=26, NA=25, NI=24, NII=23, RenA.ZMA_9377/1749-1757, RenA.ZMA_9379/1759-1768, RenA.ZMA_9151/535-538, RenA.ZMA_9339/a,e,f; *Triturus pygmaeus* Wolterstorff, 1905, Southern marbled newt, NC=13, NA=13, NI=13, NII=13, RenA.ZMA_9087/40-44, RenA.ZMA_7677/11-18.

Appendix II. The configuration of 35 three-dimensional landmarks identified on the cranium and 14 three-dimensional landmarks identified on the atlas and first and second trunk vertebrae of Salamandrid newts. For visualization of landmarks see Figure 2.

Structures	Landmark	Position
Cranium	1	The most anterior point of premaxilla
	2, 3	Premaxilla / maxilla suture
	4, 5	Maxilla / nasal suture
	6, 7	Tip of maxilla
	8, 9	Prefrontal / frontal suture
	10, 11	Lateral process of frontal (*processus alaris frontalis)*
	12	Suture between frontal and parietal
	13, 14	Posterior end of parietal
	15, 16	Tip of squamosal process
	17, 18	Orbitosphenoid / parietal suture
	19, 20	Squamosal / oticooccipital, most posterior suture
	21, 22	Quadrate, most lateral jaw point
	23, 24	Tip of the pterygoid
	25, 26	Vomerine teeth - anterior
	27, 28	Vomerine teeth - posterior
	29, 30	*Fenestra ovalis*
	31, 32	Vomer / orbitosphenoid
	33, 34	Occipital condyle
	35	Posterior paraspehenoid
Atlas	1	Tip of processus odontoideus
	2, 3	Maximal constriction of processus odontoideus
	4, 5	Most lateral point of occipital joint
	6, 7	Tip of the lamina
	8	Tip of the vertebra on the dorsal side
	9, 10	Maximal constriction of vertebra
	11, 12	Maximal curvature of the postzygapophysis
	13	The end of vertebra on the dorsal side
	14	Tip of the cotylus
First and second trunk vertebrae	1	Tip of the vertebra on the dorsal side
	2, 3	The most proximal point of the prezygapophysis
	4, 5	Maximal constriction of the vertebra at the level of transversal processes
	6, 7	The distal tips of the upper rib-bearers
	8, 9	Maximal curvature of the postzygapophysis
	10	The end of vertebra on the dorsal side
	11, 12	The distal tips of the lower rib-bearers
	13	The anterior tip of the condylus
	14	Tip of the cotylus

Appendix III. Results of Procrustes ANOVA for repeated measurements in *Triturus* species. Ind = between individual variation; Side = Directional asymmetry, Ind * Side – Fluctuating asymmetry; ME – Measurement error; SS – sum of squares; MS – mean squares; df – degrees of freedom; F – F value.

Structure	Effect	SS	MS	df	F	p
Cranium	Ind	1.25405	0.000220	5750	9.07	0.0001
	Side	0.00657	0.000140	48	5.69	0.0001
	Ind * Side	0.13280	0.000024	5520	3.08	0.0001
	ME	0.08894	0.000008	11368		
Atlas	Ind	3.32471	0.001270	2622	5.86	0.0001
	Side	0.01899	0.001190	16	5.49	0.0001
	Ind * Side	0.47765	0.000220	2208	199.05	0.0001
	ME	0.00525	0.000001	4830		
First trunk	Ind	2.86294	0.001130	2527	5.59	0.0001
	Side	0.01393	0.000870	16	4.3	0.0001
	Ind * Side	0.43102	0.000200	2128	188.81	0.0001
	ME	0.00503	0.000001	4690		
Second trunk	Ind	2.07881	0.000930	2242	4.82	0.0001
	Side	0.00661	0.000410	16	2.15	0.0052
	Ind * Side	0.36342	0.000190	1888	156.4	0.0001
	ME	0.00513	0.000001	4165		

Appendix IV

Percentages of the allometric shape changes explained by multivariate regressions of shape variables on size and the statistical significances. *** $p<0.001$; **$p<0.01$; *$p<0.05$, ns $p>0.05$.

	Static allometry				Evolutionary allometry	
Shape variables	Symmetric		Asymmetric		Independent contrasts	
	% variance explained	p	% variance explained	p	% variance explained	p
Cranium	3.6	***	0.8	ns	18.8	*
Atlas	13.8	***	0.5	ns	19.7	***
First trunk	10.4	***	0.5	ns	19.8	**
Second trunk	8.5	***	0.8	ns	16.5	**

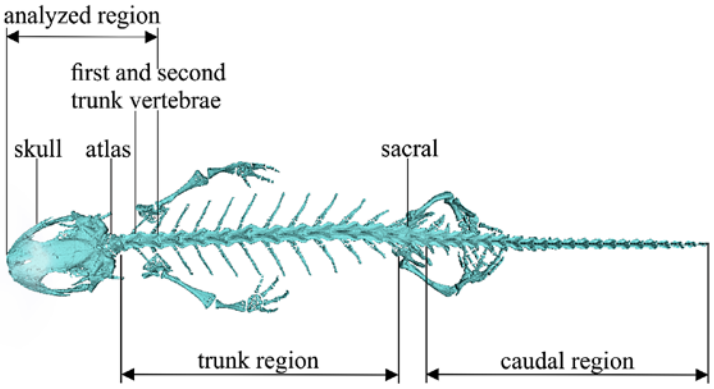

Figure 1. Regional differentiation of the vertebral column in salamandrid salamanders. The analyzed structures are marked on the 3D-model of a *Ichthyosaura alpestris* skeleton.

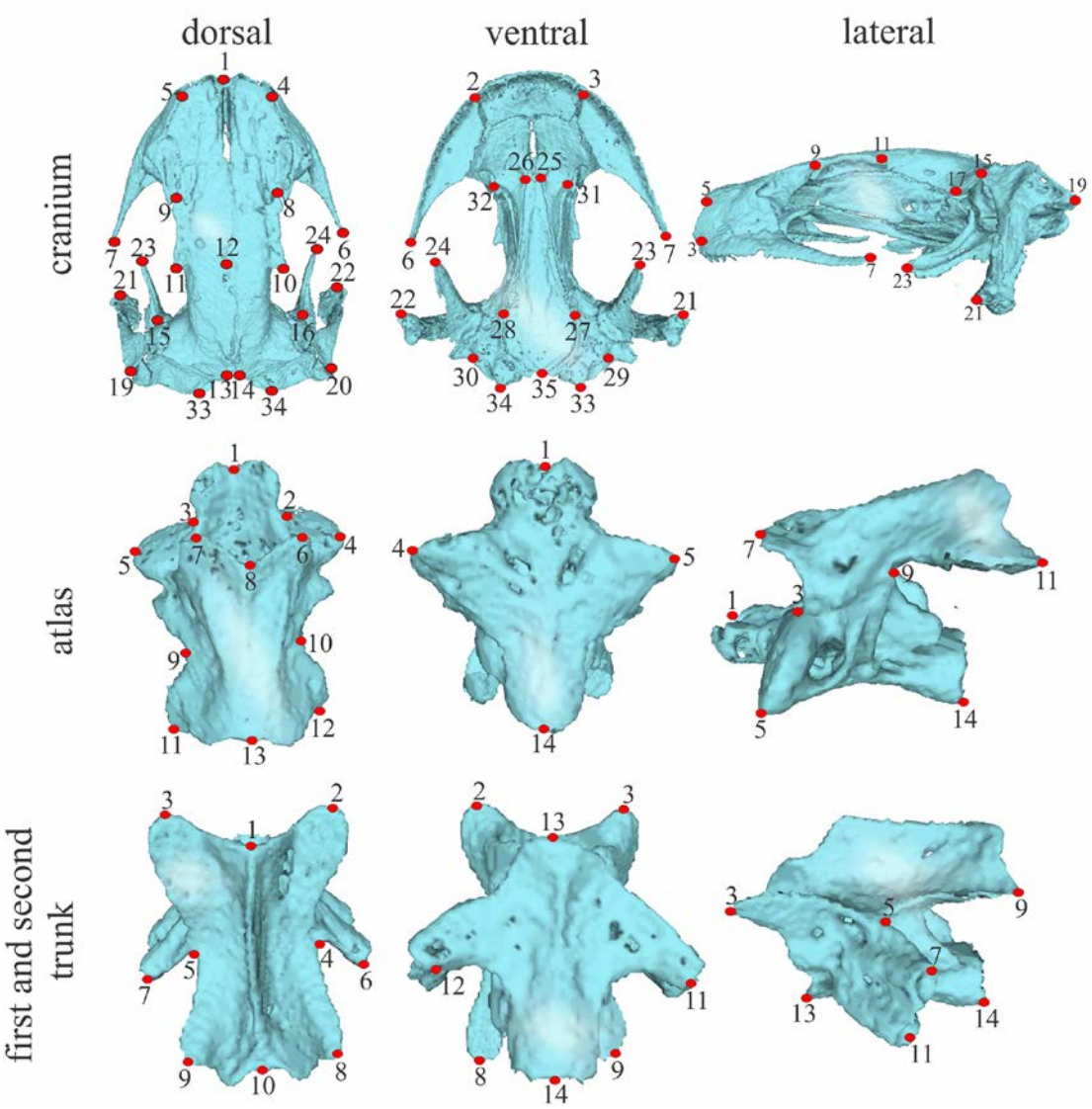

Figure 2. Three-dimensional surface models of the cranium, atlas and the first two trunk vertebrae, with superimposed landmarks. Descriptions for landmarks digitized on each structure are shown in Appendix II.

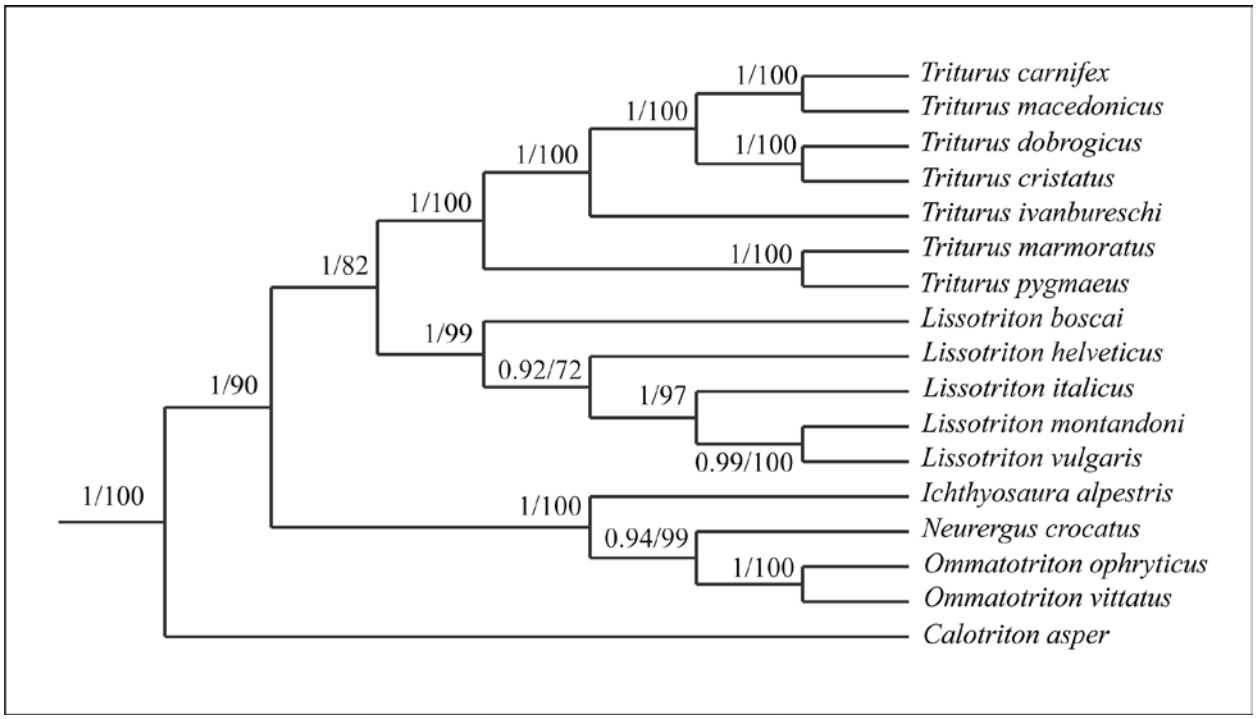

Figure 3. Phylogenetic relationships of 17 species of salamandrid salamanders figuring in the present study. The tree is compiled from data by Pabijan et al. (2015, 2017), Veith et al. (2018) and Wielstra et al. (2019) (details see text).

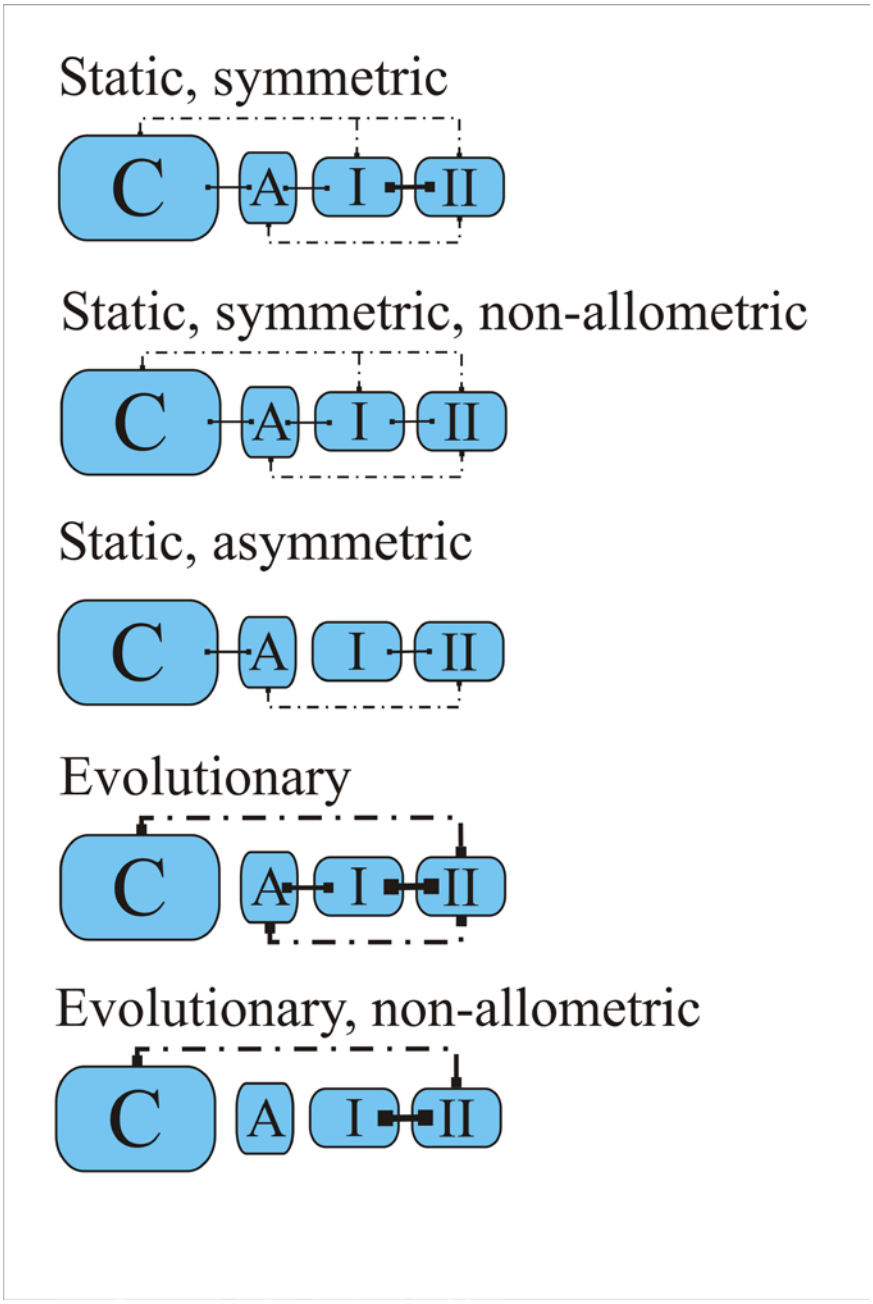

Figure 4. Patterns of morphological integration of the cranium and homologous series of vertebrae at static, developmental and evolutionary levels. For the static and evolutionary level patterns are given before and after correction for allometry. C – cranium, A – atlas, I – first trunk vertebra, II – second trunk vertebra. Thin lines represent weak integration (RV<0.5), medium thick lines represent medium integration (0.50<RV<0.75) and thick lines represent strong integration (RV>0.75). Solid lines represent integration between adjacent structures, dashed lines represent integration between separated elements.

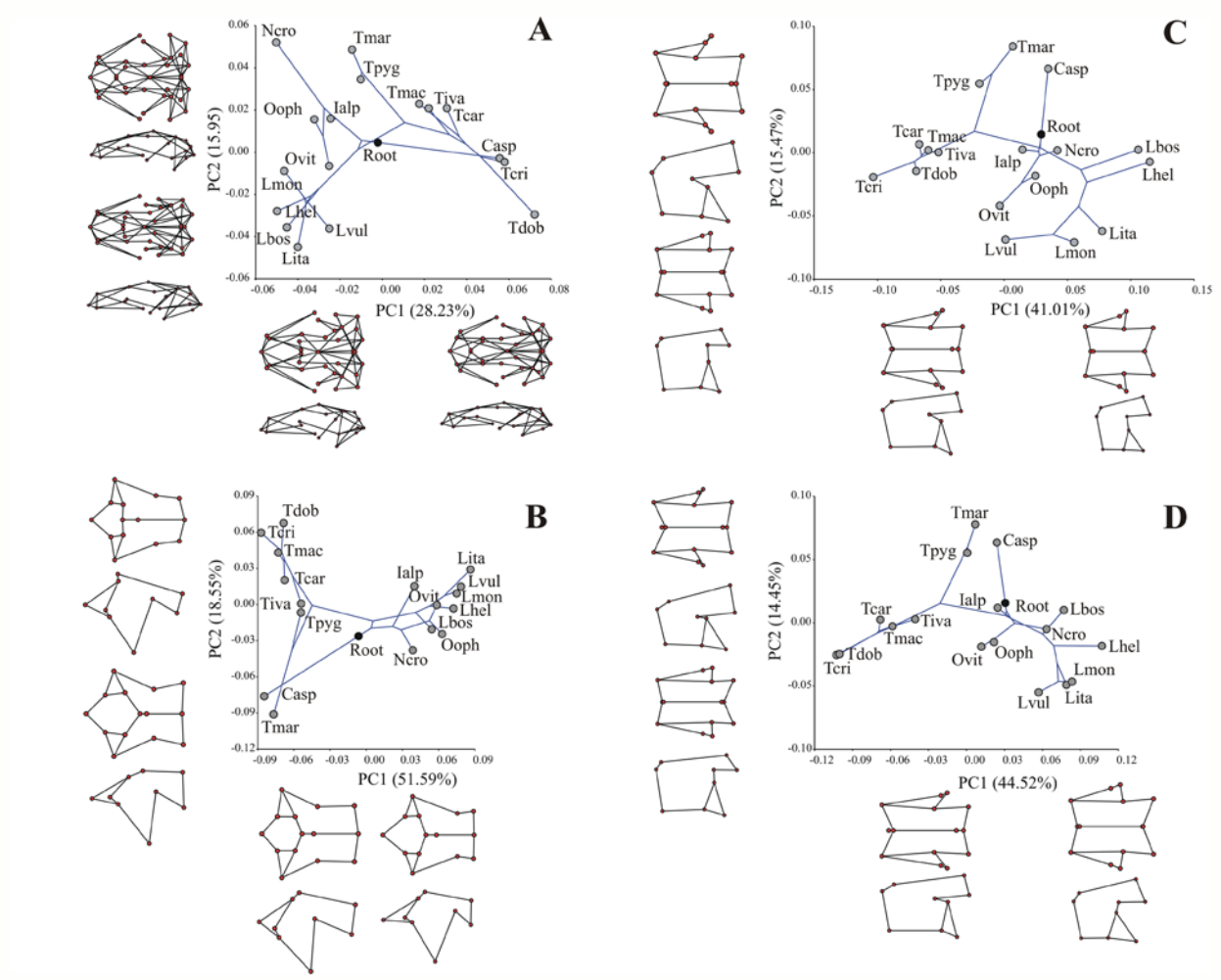

Figure 5. Phylomorphospace of the cranium (A), atlas (B), first (C) and second trunk vertebrae (D), over the first and second principal component axis, for the symmetric component of shape variation, allometric component included. The shape changes corresponding to maximal PC-scores are presented as wireframe graphs for dorsal and lateral projection along each axis. Species names are abbreviated as : Casp - *Calotriton asper*, Ialp - *Ichthyosaura alpestris*, Lbos - *Lissotriton boscai*, Lhel - *Lissotriton helveticus*, Lita - *Lissotriton italicus*, Lmon - *Lissotriton montandoni*, Lvul - *Lissotriton vulgaris*, Ooph - *Ommatotriton ophryticus*, Ovit - *Ommatotriton vittatus*, Ncro - *Neurergus crocatus*, Tcar - *Triturus carnifex*, Tcri - *Triturus cristatus*, Tdob - *Triturus dobrogicus*, Tiva - *Triturus ivanbureschi*, Tmac - *Triturus macedonicus*, Tmar -*Triturus marmoratus*, Tpyg - *Triturus pygmaeus.*